

Influence of crystal structure, ligand environment and morphology on Co *L*-edge XAS spectral characteristics in cobalt compounds

D. K. Bora,^{a,*} X. Cheng,^{a,b,c} M. Kapilashrami,^a P. A. Glans,^a Y. Luo^{b,c} and J.-H. Guo^{a,d,*}

Received 17 April 2015

Accepted 14 September 2015

Edited by R. W. Strange, University of Liverpool, UK

* Currently at Laboratory for High Performance Ceramics, Empa, Swiss Federal Laboratories for Materials Science and Technology, CH-8600 Dübendorf, Switzerland.

Keywords: cobalt *L*-edge; NEXAFS; branching ratio; site symmetry; $I(L_3)/I(L_2)$ ratio.

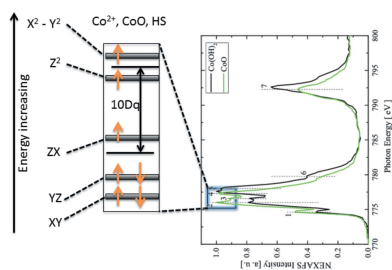
Supporting information: this article has supporting information at journals.iucr.org/s

^aAdvanced Light Source, Lawrence Berkeley National Laboratory, 1 Cyclotron Road, Berkeley, CA 94720, USA, ^bHefei National Laboratory for Physical Sciences at the Microscale, University of Science and Technology of China, Hefei, People's Republic of China, ^cDepartment of Theoretical Chemistry, School of Biotechnology, Royal Institute of Technology, SE-10691 Stockholm, Sweden, and ^dDepartment of Chemistry and Biochemistry, University of California at Santa Cruz, Santa Cruz, CA 95064, USA. *Correspondence e-mail: debajeet.bora@empa.ch, jguo@lbl.gov

The electronic structure of a material plays an important role in its functionality for different applications which can be probed using synchrotron-based spectroscopy techniques. Here, various cobalt-based compounds, differing in crystal structure, ligands surrounding the central metal ion and morphology, have been studied by soft X-ray absorption spectroscopy (XAS) at the Co *L*-edge in order to measure the effect of these parameters on the electronic structure. A careful qualitative analysis of the spectral branching ratio and relative intensities of the L_3 and L_2 peaks provide useful insight into the electronic properties of compounds such as CoO/Co(OH)₂, CoCl₂·6H₂O/CoF₂·4H₂O, CoCl₂/CoF₂, Co₃O₄ (bulk/nano/micro). For further detailed analysis of the XAS spectra, quantitative analysis has been performed by fitting the spectral profile with simulated spectra for a number of cobalt compounds using crystal field atomic multiplet calculations.

1. Introduction

Understanding the electronic structure of transition metal compounds finds profound interest in the development of synchrotron X-ray spectroscopy techniques. Cobalt-based compounds are well studied by X-ray absorption spectroscopy (XAS) to account for the electronic structural changes during its operation as a catalyst, battery *etc.* Cobalt exists in nature in two main oxidation states, namely +2 and +3. It is stable to atmospheric oxygen and, when heated at high temperatures, metallic cobalt is converted into Co₃O₄ with CoO as the final end product (IARC Monographs, 1991). It also shows magnetic properties, and a single crystal of cobalt shows magnetic anisotropy up to about 250°C (Donaldson *et al.*, 1986). The majority of cobalt-based compounds for commercial purposes exist in the +2 oxidation state with the exception of Co₂O₃ which exists in the +3 oxidation state. The oxides of cobalt such as CoO, Co₂O₃ and Co₃O₄ are used in magnetism studies (Wu *et al.*, 2011) and as catalysts for water splitting reactions (Xi *et al.*, 2012). Besides these, Co₃O₄ nanotubes are also employed as a battery material (Du *et al.*, 2007). Another analogue, cobalt hydroxide, is found to be a bright candidate for rechargeable Li-ion batteries, thermo-electric and gas sensing (Chen *et al.*, 2008; Alcántara *et al.*, 1999; Terasaki *et al.*, 1997; Frost & Wain, 2008). Cobalt-based halides are also found to be useful as a catalyst material for photoelectrochemical water splitting reactions (Kay *et al.*, 2006).



© 2015 International Union of Crystallography

With the help of synchrotron-based X-ray sources an XAS spectrum can be originated by exciting an electron from the core level of matter to the next available energy level. Owing to its dependence on the energy of the incoming beam we need a monochromatic light source in order to make an XAS spectrum element-specific. Soft X-ray absorption spectroscopy studies of the Co *L*-edge enable the electronic structures of cobalt-based oxides to be determined and also provide information about the unoccupied molecular orbitals by analysis of the intense absorption peaks of Co *L*-edge XAS spectra (Yoon *et al.*, 2002; Magnuson *et al.*, 2002; Butorin *et al.*, 2000). The *L*-edges are usually sensitive to the oxidation state, spin state and changes in the ligand field. Much information can be gained from the *L*_{2,3}-edge spectra. The intense absorption peaks originate from the dipole allowed $2p \rightarrow 3d$ transition and are usually located in the 400–1000 eV range. In this case sharp multiplet structures have been observed due to the smaller line widths than the near-edge region of transition metal *L*-edges (Butorin *et al.*, 2000; van Elp *et al.*, 1994). Dipole transitions between the core $2p$ level and unoccupied $3d$ states dominate the absorption spectrum and the local electronic structure has the same influence as a result of Coulomb interaction (van der Laan & Kirkman, 1992). The *L*-edge spectrum consists of two edges, namely *L*₃ and *L*₂, separated by about 16 eV due to core level spin–orbit splitting of the $2p_{3/2}$ and $2p_{1/2}$ orbitals (Liu *et al.*, 2007). Interpretation of the changes in symmetry can be carried out with the help of atomic multiplet calculations. In the calculation procedure the interaction between the $2p$ core hole and $3d$ valence electrons is generally considered and the *L*_{2,3}-edges are described by $2p^6 3d^n \rightarrow 2p^5 3d^{n+1}$ transitions, where $2p$ stands for transitions involving the $2p$ core hole followed by the fingerprint of available final states for every $3d^N$ initial state (de Groot *et al.*, 1990).

The need of the current study is based on the accompanying facts and answers obtained in earlier works of cobalt electronic structure studies. From recent concise accounts of Co *L*-edge XAS spectra of various systems (van Elp *et al.*, 1991; van Schooneveld *et al.*, 2012; Miedema *et al.*, 2011; He *et al.*, 2013; Iablokov *et al.*, 2012; Zheng *et al.*, 2011; Herranz *et al.*, 2009; Alayoglu *et al.*, 2011; Tuxen *et al.*, 2013; Morales *et al.*, 2004; Lin *et al.*, 2010; Knupfer *et al.*, 2006; Karvonen *et al.*, 2010; Uchimoto *et al.*, 2001; Valkeapää *et al.*, 2007; Milewska *et al.*, 2014; Tamenori, 2013; de Groot *et al.*, 1993; Kikas *et al.*, 1999; Kumagai *et al.*, 2008; Bazin *et al.*, 2000) it is evident that a good reference data set is often needed to compare the changes in the spectral characteristics of these compounds for different applications. For example, it has been contemplated that the Co *K*-edge XAS spectrum of CoO nanocrystals and bulk single crystals showed a spectrum sensitive to an octahedral field (van Elp *et al.*, 1991). To understand this, a model standard data set is required in order to acquire data necessary to understand spectral characteristics in correlation with the site symmetry of the material of interest. Similarly, these reference data sets can be helpful further to better understand the results obtained from changes in the oxidation state of the cobalt atom in a metallo-organic complex in response to

oxygen binding (van Schooneveld *et al.*, 2012; Miedema *et al.*, 2011), catalytic action of cobalt metallic and bimetallic nanoparticles (He *et al.*, 2013; Iablokov *et al.*, 2012; Zheng *et al.*, 2011; Herranz *et al.*, 2009; Alayoglu *et al.*, 2011), high-temperature catalysis during the Fischer–Tropsch reaction (Tuxen *et al.*, 2013) and electrochemical lithiation and delithiation of cobalt-based layered alkali compounds (Morales *et al.*, 2004; Lin *et al.*, 2010; Knupfer *et al.*, 2006; Karvonen *et al.*, 2010; Uchimoto *et al.*, 2001; Valkeapää *et al.*, 2007; Milewska *et al.*, 2014).

Following on from the above, the motivation of the current work is to produce a reference database of cobalt *L*-edge spectra by investigating standard cobalt compounds. This will help understand further the electronic structure of other cobalt-based functional systems with more clarity when the spectral shape and energy position differ. To achieve this we present herein systematic synchrotron-based Co *L*-edge XAS studies (Advanced Light Source/Lawrence Berkeley National Laboratory) on the correlation between the local electronic structure and crystal structure/site symmetries [CoO/Co(OH)₂; CoCl₂·6H₂O/CoF₂·4H₂O], ligand types (CoCl₂/CoF₂) and morphology (Co₃O₄: bulk, micro and nano). Although a few of these spectra have been documented in the literature, the branching ratio and the ratio of the spectral intensity have not been shown previously. Most of the spectra [CoO/Co(OH)₂; CoCl₂·6H₂O/CoF₂·4H₂O], ligand types (CoCl₂ and CoF₂) and morphology (Co₃O₄: bulk, micro and nano) discussed here are not seen in the literature besides the sets of CoO and Co₃O₄; CoF₂ and CoF₃; and LiCoO₂ (de Groot *et al.*, 1990, 1993; Tuxen *et al.*, 2013; Milewska *et al.*, 2014; Tamenori, 2013; Kikas *et al.*, 1999; Kumagai *et al.*, 2008).

2. Materials and methods

All the cobalt compounds investigated in this study were of reagent grade with 99.9% purity from Sigma Aldrich, USA. For the morphology dependent study, we have taken three Co₃O₄ samples: bulk particles, nano-size particles (<50 nm) and micrometre-size particles (<10 μm). Co *L*-edge XAS were measured at BL 8.0.1 to determine the unoccupied density of states in the Co complexes. The photon flux was 10¹² photons s⁻¹ and the glancing angle between the incident photon beam and sample surface was <10°. The pressure of the analysis chamber was 8.2 × 10⁻¹⁰ Torr.

The data were recorded in the surface-sensitive (<10 nm) total electron yield (TEY) detection mode, with a spectral resolution of 0.2 eV. The photon energy was calibrated using a Co metal foil reference sample [$2p \rightarrow L_3$ -edge peak position of the Co foil at 776.2 eV (Thompson *et al.*, 2009)]. At the initial stage of processing the spectra, these are normalized after background subtraction to a specified intensity (0, 1) value in the edge (772 eV) and ionization continuum (800 eV). After this, we normalized the spectra to the same height to enable comparison with clarity. The simulated XAS spectra for CoF₂ multiplet simulation were obtained using atomic multiplet theory and the Cowan code. The multiplet calculation method is a series of developments by many different

researchers since the late-1960s based on the Cowan–Butler–Thole code. In addition, the *CTM4XAS* software package was recently developed by F. M. F. de Groot. In this package, the effect of the crystal field is considered by the application of symmetry branching methods based on group theory. The charge transfer effect is also considered for simulating the *L*-edge spectrum and this includes the configurations of initial and final states (Cowan, 1968, 1981; Thole *et al.*, 1988; Stavitski & de Groot, 2010). For the simulation of CoO, Co(OH)₂ and anhydrous CoCl₂, atomic multiple simulations for Co(II) were performed using the *CTM4XAS 5.0* program, including full spin–orbit coupling and crystal field effects (Thompson *et al.*, 2009; Stavitski & de Groot, 2010).

3. Results and discussion

3.1. Effect of crystal structure on spectral shape, energy shift and intensity of absorption edges

3.1.1. CoO and Co(OH)₂. To observe the effect of crystal structure with distorted symmetry on the spectral characteristics we have compared the *L*-edge spectra of Co(OH)₂ and CoO. Here we have seen spectral features similar to those of the Co *L*-edge spectrum of CoO. The Co(OH)₂ spectrum consists of a multiplet peak followed by splitting of the main edge peak into four sub-peaks and a distinct charge-transfer shoulder peak, as shown in Fig. 1. First, we focus on the shape and position of the *L*₃-edge as it is well resolved in comparison with the *L*₂-edge. It provides information about the valence of the metal atom and hybridization of the metal and ligand orbitals in terms of the *t*_{2g} and *e*_g orbital signatures. Besides this, the *L*₃-edge shows more structure in comparison with the *L*₂-edge (Tuxen *et al.*, 2013) and shows good agreement with multiplet simulation with respect to the *L*₂-edge. During the data treatment, the variation of the spectral intensities has been considered with respect to the change in energy position and its magnitude. Here, the Co *L*-edge spectral energy position from a standard cobalt-based reference compound

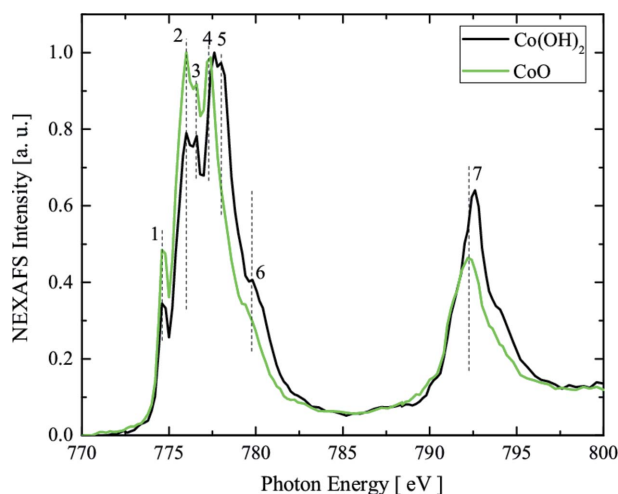


Figure 1
Co *L*-edge XAS spectra of CoO and Co(OH)₂.

Table 1

Comparison of the absorption energy positions of prominent spectral peaks of different cobalt-based compounds.

Compound	Multiplet peak energy position	Shoulder energy position	Reference
CoO	774.5 eV	780 eV	This Study
	772.5 eV	777.5 eV	de Groot <i>et al.</i> (1990)
	776 eV	780 eV	de Groot <i>et al.</i> (1993)
	777.9 eV	781 eV	Mizuno (1961)
	776 eV	780 eV	van Elp <i>et al.</i> (1991)
Co ₃ O ₄	776.2 eV	782 eV	Penfold & Taylor (1960)
	776 eV	781 eV	This study
Na _{0.4} CoO ₂	779.25 eV	782.5 eV	Morales <i>et al.</i> (2004)
	776 eV	781 eV	Wu <i>et al.</i> (2005)

has been used for the calibration of the energy scale. In this particular case all spectra have been taken in total electron yield mode so the contribution of ligand spectral characteristics is obvious but is not studied in detail. The focus here is predominantly on the Co *L*-edge spectral characteristics of different cobalt compounds.

We have found that the spectrum of CoO consists of one multiplet peak at 774.5 eV followed by splitting of the main peak into three sub-peaks along with a shoulder at 780 eV. We have also compared the energy positions and spectral shape of the Co *L*-edge spectra from CoO with those published elsewhere. This is depicted in Table 1. It is evident that the energy positions are shifted by 2–3 eV in the case of CoO in comparison with published literature results. But in our case, the reference value was correct. We have calibrated the spectra by taking good care of the cobalt reference compound measurement and set the energy at 776.2 eV by following Thompson *et al.* (2009).

Now, on comparing this observation with that of Co(OH)₂, we have observed substantial changes in the intensity of the absorption edges and spectral energy shift between both compounds. It is evident that the multiplet peak intensity of Co(OH)₂ (1, 2 and 3) is lower in comparison with CoO, while the main peak intensity (5) remains the same in magnitude as that of CoO with a shift of peak position to higher energy. The intensity of shoulder (6) for Co(OH)₂ is higher than that of CoO. The multiplet peaks 1, 2 and 3 originate from the electronic transition associated with the Co²⁺ site symmetry in the crystal structure of CoO and Co(OH)₂. In this instance, as the peaks are nearly paired with the CoO multiplet peaks, we suggest that Co²⁺ exists in an octahedral environment. We have noticed that the peak splits into four sub-points due to geometrical distortion of the crystal structure of charge neutral interspersing layers between two different layers of the crystal lattice. Note that cobalt hydroxide exists in both α and β phases. In this example we have studied the spectrum of β -Co(OH)₂ exemplified by its characteristic pink colour. It possesses a brucite-like origin where octahedra with Co²⁺ ions are coordinated in sixfold geometry by hydroxyl ions with shared edges and produce charge-neutral layers stacked over one another without any intercalated species (Ma *et al.*, 2006). On the other hand, geometrically, CoO consists of a central

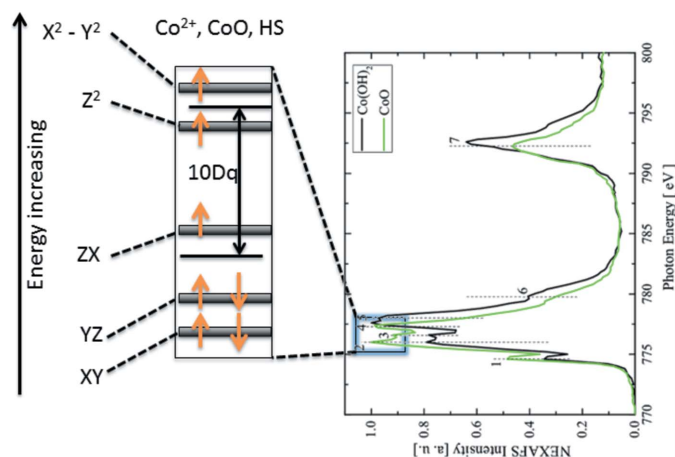
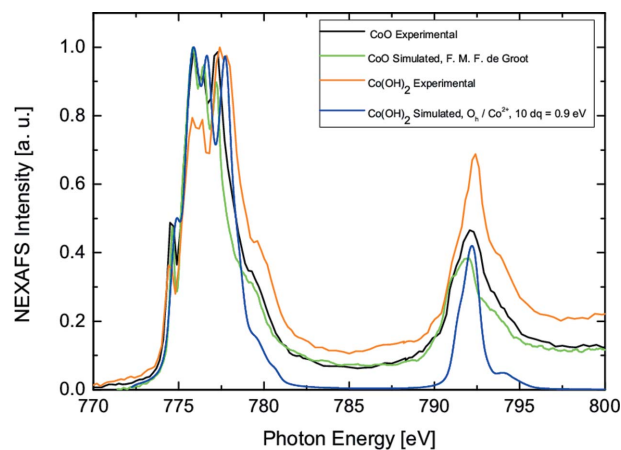
Table 2

 Variation in the relative peak intensity ratio and branching ratio between CoO and Co(OH)₂.

Sample	$I(L_3)$	$I(L_2)$	$I(L_3)/I(L_2)$	$L_3/L_2 + L_3$ (branching ratio)
CoO	1.00	0.463	2.15	0.683
Co(OH) ₂	1.00	0.6402	1.5620	0.6096

cobalt atom surrounded by six oxygen ligands with cubic octahedral symmetry. Co (I) is the octahedral site (O site) absorbing metal ion; O (I) are the six nearest octahedral oxygen ligands with bond length 2.168 Å; Co (II) are the 12 nearest metal ions and O (III) are the next neighbouring shell of oxygen atoms (Jiang & Ellis, 1996). To reach a quantitative agreement between the spectra we have also analyzed the branching ratio and the $I(L_3)/I(L_2)$ ratio as shown in Table 2. For the branching ratio analysis, spectra have been normalized to unity by taking care of the maximum intensity of the L_3 and L_2 peaks in each case.

Similar to previous reports (Park *et al.*, 2008) we find the electron occupancy in the d orbital of Co(OH)₂ to be lower in comparison with that in CoO due to the low value of the relative peak intensity ratio $I(L_3)/I(L_2)$. Similarly, the branching ratio of CoO is higher than that of Co(OH)₂ which signifies the presence of a high spin (HS) state in the case of CoO as indicated by the orbital energy level diagram (Fig. 2). A good description of the orbital energy diagram of cobalt-based compounds is described elsewhere (Bi *et al.*, 2010). The branching ratio is defined as the fraction of the intensity ratio $I(L_3)/I(L_2) + I(L_3)$ for the total transition probability involving $2p_{3/2}$ manifolds (Thole & van der Laan, 1988). If spin-orbit splitting in the valence band is neglected, one can obtain high spin states with a medium or larger branching ratio. Hereby, we have also applied the open source CTM4XAS 5.5 user interface to simulate the spectrum of CoO and Co(OH)₂ by carefully looking into the valence of the metal atom and geometrical structure of both compounds as shown in Fig. 3. The ligand or crystal field applied in both cases is the changing value of $10Dq$ or crystal field strength to simulate the spectra. We have compared the spectrum of CoO with its atomic


Figure 2
 Orbital energy level diagram of Co²⁺ (HS) ions in CoO.

Figure 3
 Comparison of the experimental and atomic multiplet simulated spectra of CoO and Co(OH)₂.

multiplet simulated spectrum by using data from F. M. F. de Groot and found close agreement with experimental spectra. In a similar manner, we have compared the spectrum of Co(OH)₂ with its atomic multiplet simulated spectrum by considering the Co²⁺ oxidation state and the presence of O_h symmetry. The $10Dq$ value of 0.9 shows a close agreement with the shape and intensity of the peak. It is the energy splitting value between e_g and t_{2g} in O_h symmetry which directly represents the crystal field strength. To account for the symmetry effect, a cubic crystal field is considered which is usually described by a single operator added to the Hamiltonian. The crystal field splitting ($10Dq$) usually represents the strength of the operator (de Groot, 1993). However, the intensity of the first two multiplet peaks in the simulated spectrum does not match that of the experimental spectrum. We believe this needs a better control of the $10Dq$ parameters to match the spectral shape. Note that in both simulated spectra the effect of $3d$ spin-orbit coupling was considered for simulating the spectral shape.

3.1.2. Comparison of CoCl₂·6H₂O with CoF₂·4H₂O: the influence of an aqueous environment. To gain further insight into the spectral characteristics due to the presence of water molecules along with a different crystal structure we have compared the spectrum of CoCl₂·6H₂O with CoF₂·4H₂O. Fig. 4 shows the Co L -edge XAS spectra of CoCl₂·6H₂O with CoF₂·4H₂O. From the results obtained we find that the spectra closely overlap each other besides an increase in the intensity of peak 5 at 779 eV. This shoulder is assigned to the charge transfer peak. Before discussing the observed modifications in the spectral features, we wish to discuss the crystal structure of both compounds under investigation. In the structure of CoCl₂·6H₂O the unit cell is monoclinic and takes two molecules. The cell parameters are $a = 10.34$ Å, $b = 7.06$ Å, $c = 6.67$ Å and $\beta = 122^\circ$ (Mizuno, 1961). Here, Co²⁺ forms crystallographic layers by the octahedral coordination of two Cl⁻ ions and water molecules in its structure, or it exists in octahedral symmetry. The crystal structure layers are parallel to (001) and it was suggested that the sub-layers stacked on top of each other parallel to the b axis and hold together by O—

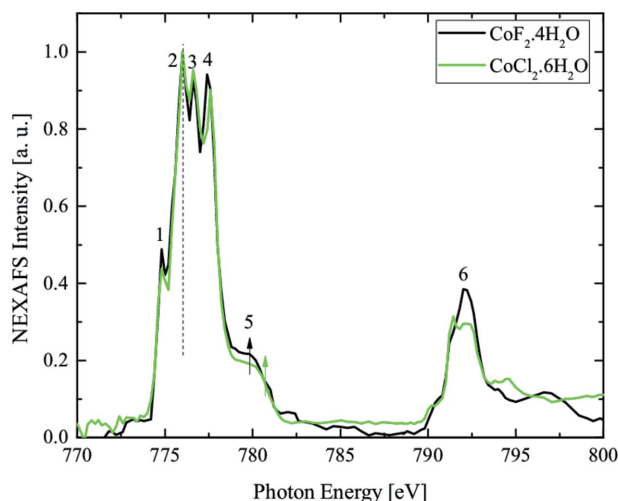


Figure 4
Co *L*-edge XAS spectra of CoF₂.4H₂O and CoCl₂.6H₂O.

H··O hydrogen bonds. On the other hand, the crystal structure of CoF₂.4H₂O is trigonal or distorted octahedron. The unit cell is a disordered hexagonal cell with cell parameters $a = 9.50 \text{ \AA}$, $b = 4.82 \text{ \AA}$. The structure is confirmed by that of FeF₂.4H₂O whereby the Fe(H₂O)₄F₂ group is randomly oriented over 12 potential sites for H₂O and F (Penfold & Taylor, 1960). In this case, Co²⁺ ions are thought to be in *D*_{3d} symmetry.

In the following we discuss the influence of the different symmetry of the Co *L*-edge XAS spectrum for both compounds. From the XAS spectrum it is apparent that the spectrum of CoCl₂.6H₂O closely matched that of CoO and anhydrous CoCl₂ as shown in Figs. 1 and 5. This further corroborates the presence of the Co²⁺ state in octahedral symmetry. The only deviation in this instance is the *L*₂ peak splitting. The charge transfer peak is well developed in the case of CoCl₂.6H₂O with respect to CoF₂.6H₂O, while in the latter case it is more pronounced. This may be linked to the

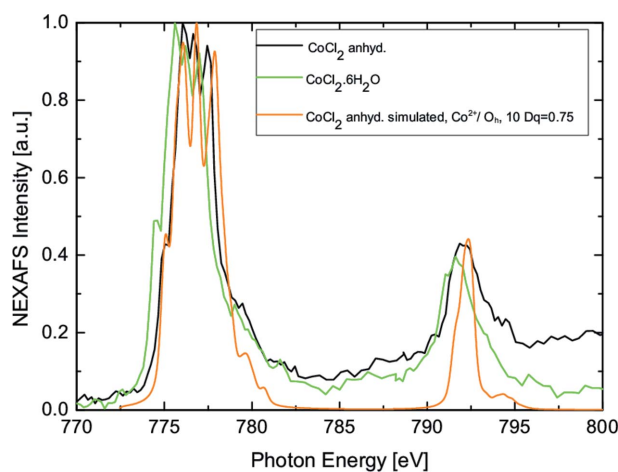


Figure 5
Comparison of Co *L*-edge XAS spectrum of CoCl₂ and CoCl₂.6H₂O with the atomic multiplet simulated spectrum obtained using CTM4XAS 5.5. Software from F. M. F. de Groot.

Table 3

Variation in the relative peak intensity ratio and branching ratio calculation for spectra of CoF₂.4H₂O and CoCl₂.6H₂O.

Sample	$I(L_3)$	$I(L_2)$	$I(L_3)/I(L_2)$	$L_3/L_2 + L_3$ (branching ratio)
CoF ₂ .4H ₂ O	1.00	0.3849	2.5980	0.7220
CoCl ₂ .6H ₂ O	1.00	0.3144	3.1806	0.7611

presence of *D*_{3d} symmetry where the electronic transition will differ from CoCl₂.6H₂O with *O*_h symmetry. A similar case has been found for Na_xCoO₂ (Wu *et al.*, 2005). Here the influence of the *D*_{3d} symmetry of the Co *L*-edge XAS spectra was taken into account and it was resolved that the compound showed charge transfer electronic behaviour rather than a Mott–Hubbard character. The electronic transition in this case will involve transition to the higher number of unoccupied states. On the other hand, the *d* orbital occupancy increases in the case of CoCl₂.6H₂O as the $I(L_3)/I(L_2)$ ratio is higher (Table 3) and also Co²⁺ exists in the high spin state supported by a higher branching ratio. However, following the work of Tamenori (2013), we have compared the spectrum of anhydrous CoCl₂ and hydrated CoCl₂ (Fig. 5). In both cases we find the same characteristics in terms of spectral features which leads us to conclude that the hydrated CoCl₂ becomes dried out in UHV as discussed by Tamenori (2013). After all, we agree upon the fact that hydrated CoCl₂ dried out and maintains the Co²⁺ oxidation state as discussed elsewhere. For a closer look at the spectral features the anhydrous and hydrated spectra of CoCl₂ are compared with the atomic multiplet simulated spectrum by considering the possession of an octahedral symmetry and Co²⁺ oxidation state. The simulated spectra have shown all the characteristic peak shapes; however, there is some shift in the peak at 777.5 eV. A 10*Dq* value of 0.75 is used for the simulation. The hydrated spectrum also showed similar peak features as that of the simulated spectrum, revealing the anhydrous nature of CoCl₂ instead of the presence of water molecules. We have also found that the spectrum of CoO is broadened with respect to CoCl₂. By careful inspection of the magnified *L*₃-edge (Fig. S1 of the supporting information), it can be seen that the intensity of the multiplet peak (1) in the case of CoO is becoming higher in comparison with CoCl₂ (1'). For CoO, the main peak intensity at position 4 is also becoming higher with an enhance spectral weight transfer at position 5 signifying that CoO is better conducted or has increased charge transfer properties in comparison with CoCl₂. In an octahedral symmetry the arrangement of ligand atoms around the central metal atoms splits the *t*_{2g} and *e*_g orbitals. The *e*_g orbitals have the highest energy and contain holes with parallel spins (Park *et al.*, 2008). Splitting of the main peak in both cases can be ascribed to this phenomenon.

Changes in the spectra in spite of having the same symmetry may also be an indication of the presence of high-spin and lower-spin Co²⁺. Note that an abrupt change in the spectra normally occurs and this is an indication of a high-spin to low-spin transition (van Elp *et al.*, 1994). In this example this is

validated from the difference in branching ratio as shown in Table S4 of the supporting information.

3.2. Effect of ligands around the metal centres on the spectral features: comparison of CoCl_2 and CoF_2

In parallel to the above example, we have compared the spectra of CoCl_2 and CoF_2 in order to determine the effect of the ligand surrounding the central metal ion on the spectral characteristics. The bearing of a ligand surrounding the metal cation or cobalt ions with different electronegativity can also affect the spectral shape in terms of formation of new multiplet features. To validate this, we have compared the experimental Co L -edge spectra of CoCl_2 and CoF_2 as shown in Fig. 6(a). For a qualitative understanding of the spectral shape, we first discuss the characteristic site symmetry of each individual compound. From the structural point of view CoF_2 has D_{2h} or tetragonal symmetry (Costa *et al.*, 1993) whereas CoCl_2

is octahedral or has O_h symmetry. In the crystal structure of CoCl_2 the Cl atoms pack themselves in a cubic-close-packing arrangement and Co atoms belong to the available tetrahedral groups of Cl atoms. Here, Cl atoms are combined with three Co atoms and form a layer structure parallel to (111). The structure is also isomorphic with that of CdCl_2 (Grime & Santos, 1934).

A magnification of the L_3 -edge is shown in Fig. 6(b). Note that the multiplet peak (1) for CoF_2 increases in intensity in comparison with CoCl_2 , whereas the main point at position (4) has a reduction in peak intensity. The charge transfer peak at position (5) is higher in intensity in comparison with CoCl_2 . Note that this small change in the spectrum resulted from the different proportions of each compound. This extra enhancement in the multiplet feature for CoF_2 may be a result of a decrease in the near-edge multiplet splitting due to an increased anion or ligand electronegativity (van der Laan *et al.*, 1986). This aids in the shake up of the charge transfer multiplet peak.

Comparison of the experimental and atomic multiplet simulated spectra shows that there is a good match for both compounds except for the charge transfer shoulder peaks [Figs. 7(a) and 7(b)]. During the calculation a cubic crystal field was included which renders a full correspondence with the spectral details. The simulations were carried out by utilizing the crystal-field multiplet calculation. The symmetry used in the calculation to represent the crystal field effect is O_h for CoCl_2 and D_{2h} for CoF_2 . The Slater–Condon integrals were scaled by 0.80 to calculate the absorption spectrum. The simulated spectra have been met well with the inclusion of $3d$ spin–orbit coupling which further improved the total spectral shape and branching ratio for CoF_2 . This is also observable in our case from the simulated branching ratio (Table 4). For the experimental spectrum of anhydrous CoCl_2 it is simulated with an optimized $10Dq$ parameter of 0.75 and setting the Lorentzian and Gaussian broadening to 0.15 (Fig. 7b).

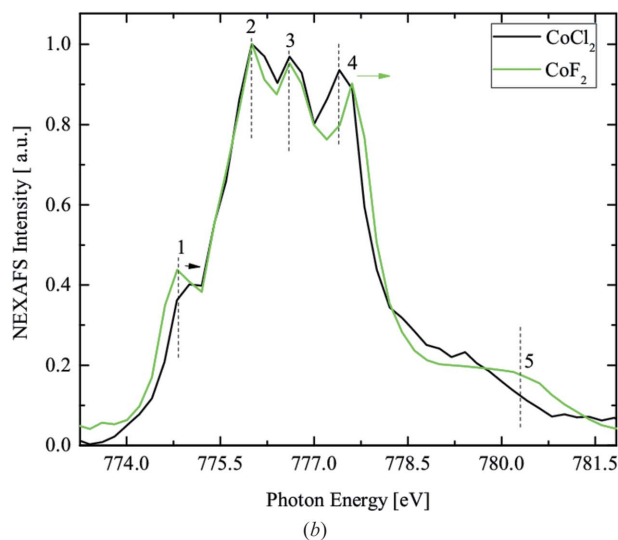
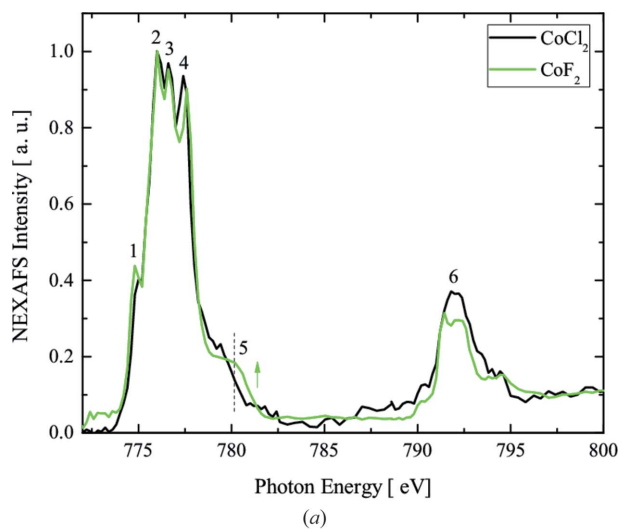


Figure 6
(a) Comparison of the Co L -edge XAS ($2p \rightarrow 3d$ transitions) of CoF_2 and CoCl_2 . (b) Detailed presentation of the spectral features in the low-energy range.

3.3. Effect of morphology on the spectral shape of Co_3O_4 (bulk, micro- and nano-size)

The electronic structure of materials in different morphological form can shed light on its correlation with the surface oxidation state. We have compared the spectrum of Co_3O_4 with different morphologies ranging from bulk to nano-scale as mentioned in §2. The corresponding Co L -edge XAS spectra are shown in Fig. 8. Here, Co_3O_4 has a normal spinel structure with Co^{2+} ions occupying tetrahedral sites and Co^{3+} ions occupying octahedral sites (Iablokov *et al.*, 2012). The spectrum of Co_3O_4 consists of a mixture of Co (II) and Co (III) oxidation states. A similar observation was made for Co_3O_4 under a reducing environment for Fischer–Tropsch synthesis as mentioned earlier (Morales *et al.*, 2004), and the energy positions of prominent peaks in the Co L_3 -edge are compared in Table 2. On comparing three spectra of bulk, micro-scale and nano-scale Co_3O_4 it is found that the spectral shape for both bulk and micro-size samples matched well while there is a broadening of spectra in the case of the nano-

Table 4

Variation in the relative peak intensity ratio and branching ratio calculation for spectra of CoF_2 and CoCl_2 .

Sample	$I(L_3)$	$I(L_2)$	$I(L_3)/I(L_2)$	$L_3/L_2 + L_3$ (branching ratio)
CoF_2	1.00	0.3144	3.1806	0.76080
CoCl_2	1.00	0.3712	2.693	0.729

size sample. The maximum intensities of the L_3 -edge (peak 2) closely matched, while the peak 1 intensities slightly differ in each case and for the nanoparticle sample reaches a maximum value. The lack of any energy shift indicates that the oxidation state of cobalt remains the same in all cases. The additional gain in strength of peak 1 might be due to slight changes in the geometrical structure of Co_3O_4 on going from bulk to nano. Looking into the structure of Co_3O_4 , it has a normal spinel structure with Co^{2+} ions occupying tetrahedral sites and Co^{3+} ions occupying octahedral sites. The higher intensity of peak 1 in the case of nano Co_3O_4 can be ascribed to the nano-scale

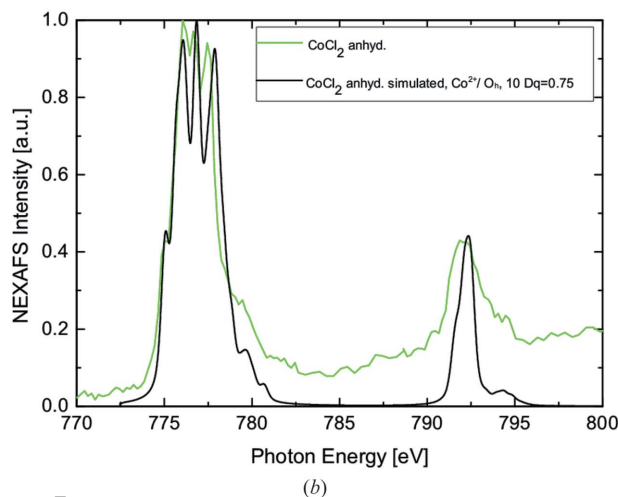
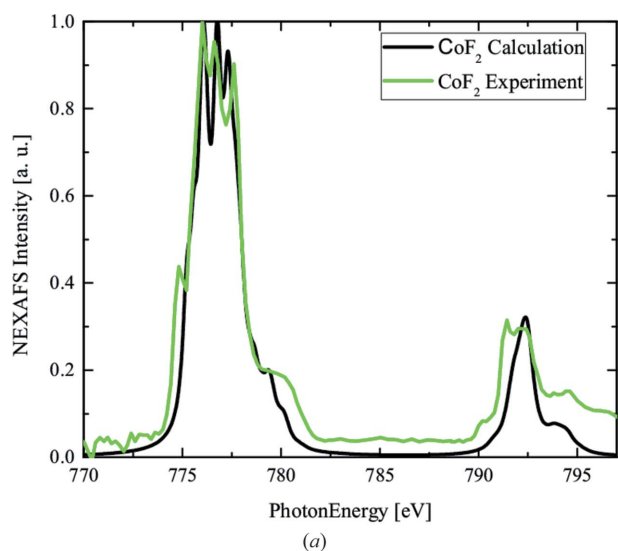


Figure 7

Comparison of the Co L -edge experimental spectra with the simulated one obtained by applying the atomic multiplet theory. (a) CoF_2 . (b) CoCl_2 .

Table 5

Variation in the relative peak intensity ratio and branching ratio calculation for the spectrum of Co_3O_4 (micro, nano and bulk).

Sample	$I(L_3)$	$I(L_2)$	$I(L_3)/I(L_2)$	$L_3/L_2 + L_3$ (branching ratio)
Co_3O_4 nano	1	0.6685	1.4958	0.60
Co_3O_4 micro	1	0.5975	1.6736	0.6259
Co_3O_4 bulk	1.00	0.621	1.612	0.61

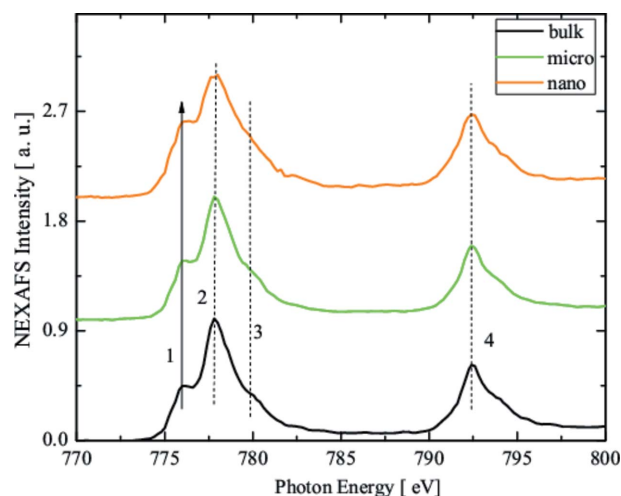


Figure 8

Co L -edge XAS comparison of bulk, micro and nano Co_3O_4 .

size effect which includes surface imperfection, surface confinement effects and surface strain anisotropies (Park *et al.*, 2008). To gain further insight into the spectral discussion, we would like to consider the $I(L_3)/I(L_2)$ ratio, the branching ratio for all the cases as shown in Table 5. The simulated $I(L_3)/I(L_2)$ ratio for all of the samples varies to some extent while a significant change has been observed for the nanoparticle. The low value of the $I(L_3)/I(L_2)$ ratio for the nanoparticle agrees quite well with the earlier observation for the Fe L -edge XAS study of the BiFeO_3 nanoparticle in comparison with the bulk (Park *et al.*, 2008). For the nanoparticle, the change in $I(L_3)/I(L_2)$ value can also be due to changes in the oxidation state from Co^{3+} to Co^{2+} on its surface.

4. Conclusion

After careful analysis of the spectral details of a series of cobalt compounds, the following conclusions can be made. Geometrical distortion in the crystal structure is found to be responsible for the observed peak splitting in the case of $\text{Co}(\text{OH})_2$. The presence of a different ligand around the central metal ion in compounds having the same symmetry also influences the spectral characteristics in a slightly different scenario. For instance, $\text{CoF}_2/\text{CoCl}_2$ and CoO/CoCl_2 systems show different spectral characteristics indicating the presence of a high-spin to low-spin transition for the Co^{2+} ion. In the case of nano-particulate Co_3O_4 the changes in the intensity ratio indicate the presence of a Co^{2+} to Co^{3+}

conversion on its surface. Finally, the present database will indirectly help scientists working in the field of materials science in terms of understanding the electronic properties of materials under different processing and experimental conditions.

Acknowledgements

The authors would like to acknowledge the funding received from the LDRD project supported by the Directorate of Berkeley Lab. The ALS is supported by the Director, Office of Science/BES, of the US DoE, No. DE-AC02-05CH11231. This research used resources of the National Energy Research Scientific Computing Center, which is endorsed by the Office of Science of the US Department of Energy under contract No. DE-AC02-05CH11231.

References

- Alayoglu, S., Beaumont, S., Zheng, F., Pushkarev, V. V., Zheng, H., Iablokov, V., Liu, Z., Guo, J., Kruse, N. & Somorjai, G. A. (2011). *Top. Catal.* **54**, 778–785.
- Alcántara, R., Lavela, P., Tirado, J. L., Zhecheva, E. & Stoyanova, R. (1999). *J. Solid State Electrochem.* **3**, 121–134.
- Bazin, D., Kovács, I., Guzzi, L., Parent, P., Laffon, C., De Groot, F., Ducreux, O. & Lynch, J. (2000). *J. Catal.* **189**, 456–462.
- Bi, L., Kim, H., Dionne, G. F. & Ross, C. A. (2010). *New J. Phys.* **12**, 043044.
- Butorin, S. M., Guo, J.-H., Wassdahl, N. & Nordgren, J. E. (2000). *J. Electron Spectrosc. Relat. Phenom.* **110–111**, 235–273.
- Chen, J. M., Hsieh, C. T., Huang, H. W., Huang, Y. H., Lin, H. H., Liu, M. H., Liao, S. C. & Shih (2008). *Synthesis of composite nanofibers for applications in lithium batteries*. US Patent 7323218 B2.
- Costa, M. M. R., Paixão, J. A., de Almeida, M. J. M. & Andrade, L. C. R. (1993). *Acta Cryst.* **B49**, 591–599.
- Cowan, R. D. (1968). *J. Opt. Soc. Am.* **58**, 808.
- Cowan, R. D. (1981). *The Theory of Atomic Structure and Spectroscopy*. University of California Press.
- Donaldson, J. D., Clark, S. J. & Gries, S. M. (1986). *Cobalt in Chemicals*. Slough: Cobalt Development Institute.
- Du, N., Zhang, H., Chen, B. D., Wu, J. B., Ma, X. Y., Liu, Z. H., Zhang, Y. Q., Yang, D. R., Huang, X. H. & Tu, J. P. (2007). *Adv. Mater.* **19**, 4505–4509.
- Elp, J. van, Peng, G., Searle, B. G., Mitra-Kirtley, S., Huang, Y. H., Johnson, M. K., Zhou, Z. H., Adams, M. W. W., Maroney, M. J. & Cramer, S. P. (1994). *J. Am. Chem. Soc.* **116**, 1918–1923.
- Elp, J. van, Wieland, J. L., Eskes, H., Kuiper, P., Sawatzky, G. A., de Groot, F. M. F. & Turner, T. S. (1991). *Phys. Rev. B*, **44**, 6090–6103.
- Frost, R. L. & Wain, D. (2008). *J. Therm. Anal. Calorim.* **91**, 267–274.
- Grime, H. & Santos, J. A. (1934). *Z. Kristallogr.* **88**, 136–141.
- Groot, F. M. F. de (1993). *J. Electron Spectrosc. Relat. Phenom.* **62**, 111–130.
- Groot, F. M. F. de, Abbate, M., van Elp, J., Sawatzky, G. A., Ma, Y. J., Chen, C. T. & Sette, F. (1993). *J. Phys. Condens. Matter*, **5**, 2277–2288.
- Groot, F. M. F. de, Fuggle, J. C., Thole, B. T. & Sawatzky, G. A. (1990). *Phys. Rev. B*, **42**, 5459–5468.
- He, Q., Cheng, X., Wang, Y., Qiao, R., Yang, W. & Guo, J. (2013). *J. Porphyrins Phthalocyanines*, **17**, 252–258.
- Herranz, T., Deng, X., Cabot, A., Guo, J. & Salmeron, M. (2009). *J. Phys. Chem. B*, **113**, 10721–10727.
- Iablokov, V., Beaumont, S. K., Alayoglu, S., Pushkarev, V. V., Specht, C., Gao, J., Alivisatos, A. P., Kruse, N. & Somorjai, G. A. (2012). *Nano Lett.* **12**, 3091–3096.
- IARC Monographs (1991). *IARC Monographs on the Evaluation of Carcinogenic Risk to Humans, IARC Monograph Vol. 52, Chlorinated Drinking-water; Chlorination By-products; Some Other Halogenated Compounds; Cobalt and Cobalt Compounds*. WHO Press.
- Jiang, T. & Ellis, D. E. (1996). *J. Mater. Res.* **11**, 2242–2256.
- Karvonen, L., Valkeapää, M., Liu, R., Chen, J., Yamauchi, H. & Karppinen, M. (2010). *Chem. Mater.* **22**, 70–76.
- Kay, A., Cesar, I. & Grätzel, M. (2006). *J. Am. Chem. Soc.* **128**, 15714–15721.
- Kikas, A., Ruus, R., Saar, A., Nömmiste, E., Käämbre, T. & Sundin, S. (1999). *J. Electron Spectrosc. Related Phenom.* **101–103**, 745–749.
- Knupfer, K. M., Geck, J., Hess, C., Schwieger, T., Krabbes, G., Sekar, C., Batchelor, D. R., Berger, H. & Büchner, B. (2006). *Phys. Rev. B*, **74**, 115123.
- Kumagai, Y., Ikeno, H., Oba, F., Matsunaga, K. & Tanaka, I. (2008). *Phys. Rev. B*, **77**, 155124.
- Laan, G. van der & Kirkman, I. W. (1992). *J. Phys. Condens. Matter*, **4**, 4189–4204.
- Laan, G. van der, Zaanen, J., Sawatzky, G. A., Karnatak, R. & Esteva, J.-M. (1986). *Phys. Rev. B*, **33**, 4253–4263.
- Lin, H.-J., Chin, Y. Y., Hu, Z., Shu, G. J., Chou, F. C., Ohta, H., Yoshimura, K., Hébert, S., Maignan, A., Tanaka, A., Tjeng, L. H. & Chen, C. T. (2010). *Phys. Rev. B*, **81**, 115138.
- Liu, H., Guo, J., Yin, Y., Augustsson, A., Dong, C., Nordgren, J., Chang, C., Alivisatos, P., Thornton, G., Ogletree, D. F., Requejo, F. G., de Groot, F. & Salmeron, M. (2007). *Nano Lett.* **7**, 1919–1922.
- Ma, R., Liu, Z., Takada, K., Fukuda, K., Ebina, Y., Bando, Y. & Sasaki, T. (2006). *Inorg. Chem.* **45**, 3964–3969.
- Magnuson, M., Butorin, S. M., Guo, J.-H. & Nordgren, J. (2002). *Phys. Rev. B*, **65**, 205106.
- Miedema, P. S., van Schooneveld, M. M., Bogerd, R., Rocha, T. C. R., Hävecker, M., Knop-Gericke, A. & de Groot, F. M. F. (2011). *J. Phys. Chem. C*, **115**, 25422–25428.
- Milewska, A., Świerczek, K., Tobola, J., Boudoire, F., Hu, Y., Bora, D. K., Mun, B. S., Braun, A. & Molenda, J. (2014). *Solid State Ion.* **263**, 110–118.
- Mizuno, J. (1961). *J. Phys. Soc. Jpn*, **16**, 1574–1580.
- Morales, F., de Groot, F. M. F., Glatzel, P., Kleimenov, E., Bluhm, H., Hävecker, M., Knop-Gericke, A. & Weckhuysen, B. M. (2004). *J. Phys. Chem. B*, **108**, 16201–16207.
- Park, T., Sambasivan, S., Fischer, D. A., Yoon, W., Misewich, J. A. & Wong, S. S. (2008). *J. Phys. Chem. C*, **112**, 10359–10369.
- Penfold, B. R. & Taylor, M. R. (1960). *Acta Cryst.* **13**, 953–956.
- Schooneveld, M. M. van, Kurian, R., Juhin, A., Zhou, K., Schlappa, J., Strocov, V. N., Schmitt, T. & de Groot, F. M. F. (2012). *J. Phys. Chem. C*, **116**, 15218–15230.
- Stavitski, E. & de Groot, F. (2010). *Micron*, **41**, 687.
- Tamenori, Y. (2013). *J. Synchrotron Rad.* **20**, 419–425.
- Terasaki, I., Sasago, Y. & Uchinokura, K. (1997). *Phys. Rev. B*, **56**, R12685–R12687.
- Thole, B. T. & van der Laan, G. (1988). *Phys. Rev. B*, **38**, 3158–3171.
- Thole, B., van der Laan, G. & Butler, P. (1988). *Chem. Phys. Lett.* **149**, 295–299.
- Thompson, A., Attwood, D., Gullikson, E., Howells, M., Kim, K.-J., Kirz, J., Kortright, J., Lindau, I., Liu, Y., Pianetta, P., Robinson, A., Scofield, J., James, U., Williams, G. & Winick, H. (2009). *X-ray Data Booklet*, 3rd ed. Berkeley: Lawrence Berkeley National Laboratory.
- Tuxen, A., Carencio, S., Chintapalli, M., Chuang, C., Escudero, C., Pach, E., Jiang, P., Borondics, F., Beberwyck, B., Alivisatos, A. P.,

- Thornton, G., Pong, W., Guo, J.-H., Perez, R., Besenbacher, F. & Salmeron, M. (2013). *J. Am. Chem. Soc.* **135**, 2273–2278.
- Uchimoto, Y., Sawada, H. & Yao, T. (2001). *J. Synchrotron Rad.* **8**, 872–873.
- Valkeapää, M., Katsumata, Y., Asako, I., Motohashi, T., Chan, T. S., Liu, R. S., Chen, J. M., Yamauchi, H. & Karppinen, M. (2007). *J. Solid State Chem.* **180**, 1608–1615.
- Wu, J., Carlton, D., Park, J. S., Meng, Y., Arenholz, E., Doran, A., Young, A. T., Scholl, A., Hwang, C., Zhao, H. W., Bokor, J. & Qiu, Z. Q. (2011). *Nat. Phys.* **7**, 303–306.
- Wu, W. B., Huang, D. J., Okamoto, J., Tanaka, A., Lin, H.-J., Chou, F. C., Fujimori, A. & Chen, C. T. (2005). *Phys. Rev. Lett.* **94**, 146402.
- Xi, L., Tran, P. D., Chiam, S. Y., Bassi, P. S., Mak, W. F., Mulmudi, H. K., Batabyal, S. K., Barber, J., Loo, J. C. & Wong, L. H. (2012). *J. Phys. Chem. C*, **116**, 13884–13889.
- Yoon, W., Kim, K., Kim, M., Lee, M., Shin, H., Lee, J., Lee, J. & Yo, C. (2002). *J. Phys. Chem. B*, **106**, 2526–2532.
- Zheng, F., Alayoglu, S., Guo, J., Pushkarev, V., Li, Y., Glans, P., Chen, J. & Somorjai, G. (2011). *Nano Lett.* **11**, 847–853.